Chemical Science

ROYAL SOCIETY OF CHEMISTRY

REVIEW

View Article Online
View Journal | View Issue

Cite this: *Chem. Sci.*, 2021, **12**, 15206

Alkali and alkaline-earth metal ion–solvent co-intercalation reactions in nonaqueous rechargeable batteries†

Lin Li, [ab] Zhe Hu, [a] Shuo Zhao [b] and Shu-Lei Chou *[a]

Alkali and alkaline-earth metal ion–solvent co-intercalation reactions have attracted extensive attention in recent years owing to the advantage of the absence of a desolvation process, which generally results in fast kinetics and good rate performance for batteries. However, less attention has been paid to summarizing the mechanism, performance and other related aspects about ion–solvent co-intercalation reaction in batteries. A summary of alkali and alkaline-earth metal ion–solvent co-intercalation reactions in nonaqueous rechargeable batteries is presented in this review, which mainly focuses on the electrochemical performance, ion–solvent co-intercalation mechanism, conditions for reversible ion–solvent co-intercalation and potential for practical application. It is suggested that future research should focus on reducing the redox potential of the ion–solvent co-intercalation reaction to achieve high energy-density and power-density full cells. This review provides an understanding of alkali and alkaline-earth metal ion–solvent co-intercalation reactions in nonaqueous rechargeable batteries and will serve as significant guidance for researchers to further develop ion–solvent co-intercalation reactions for fast-charging batteries.

Received 2nd August 2021
Accepted 4th October 2021

DOI: 10.1039/d1sc04202e

rsc.li/chemical-science

1. Introduction

According to the International Energy Outlook 2020 (IEO 2020, issued by the U.S. Energy Information Administration), world energy consumption has been increasing and will rise by nearly 50% by 2050.[1] However, the current energy supply mainly relies on fossil fuels, which are limited and non-renewable.[2] In addition, the combustion of fossil fuels will emit a large amount of greenhouse gases, which results in global warming.[3] In 2015, 195 nations made ambitious commitments to reduce their emissions of greenhouse gases.[4] It is clearer than ever that the future belongs to renewable clean energy such as wind and solar resources.[5,6] The ever-increasing demand for intermittent renewable clean energy makes it important to develop large-scale energy storage technologies.[7–10] Electrochemical energy storage technology shows great potential for large-scale energy storage systems due to their long cycle life and environmental

[a]*Institute for Carbon Neutralization, College of Chemistry and Materials Engineering, Wenzhou University, Wenzhou, Zhejiang 325035, China. E-mail: chou@wzu.edu.cn*
[b]*Key Laboratory of Advanced Energy Materials Chemistry, Ministry of Education, Renewable Energy Conversion and Storage Center, College of Chemistry, Nankai University, Tianjin 300071, China*

† Dedicated to the 100th anniversary of Chemistry at Nankai University.

Lin Li received his B.S. degree in materials science and engineering from Nanchang University (2016). He obtained his PhD from Nankai University in 2021. His research focuses on advanced materials for sodium-ion batteries and potassium-ion batteries.

Zhe Hu received his Bachelor's degree (2011) in chemistry and Master's degree (2013) in material engineering from Nankai University, China. He obtained his PhD from the Institute for Superconducting and Electronic Materials, University of Wollongong, in 2019. His research focuses on lithium-ion batteries and sodium-ion batteries.

friendliness.[11–13] Since lithium-ion batteries (LIBs) were first commercialized by Sony, LIBs have been extensively applied in portable electronic devices and electric vehicles due to their high energy density and long cycle life.[14–17] Moreover, demonstrations of their applications have been carried out in power grid peak shaving and distributed energy storage.[18] Recently, rechargeable battery systems beyond LIBs (such as sodium, potassium, magnesium, calcium, aluminum and zinc-ion batteries) have also attracted extensive attention due to their relatively high crustal abundance and potentially low-cost mass fabrication.[19–26]

To date, with the rapid development of science and technology, developing different energy storage devices with unique properties (such as high power density, high energy density, low cost and/or high safety) for specific application fields is necessary.[27,28] Among these, rechargeable batteries with high power density have attracted extensive attention because they can store/release energy quickly (in a few minutes, or even in a matter of seconds).[28,29] To realize the high-rate charging of batteries, it is important to search for some effective strategies to improve the reaction kinetics of ion intercalation.[30,31] In general, the conventional energy storage mechanism of rechargeable batteries is the insertion/extraction of naked ions into/from the host materials.[32–34] Before insertion into host materials, the ions must undergo a desolvation process, which inevitably slows the kinetics. Thus, eliminating the desolvation process would be an effective strategy to improve the reaction kinetics and thus achieve fast-rate charging batteries.

Since the Na^+–solvent co-intercalation into graphite was first reported by Adelhelm's group in 2014, the ion–solvent co-intercalation reaction has attracted increasing attention due to its unique advantages.[35] The ion–solvent co-intercalation reaction eliminates the desolvation process, which results in fast reaction kinetics and then shows outstanding rate performance. In addition, superior cycling stability is beneficial for practical application. The ion–solvent co-intercalation reaction generally exhibits a relatively high redox potential, which effectively avoids metal dendritic growth and guarantees good safety at a high rate of the charge/discharge process. No SEI layer or a thin and stable SEI layer is formed when the ion–solvent co-intercalation reaction occurs, which favours a high coulombic efficiency, good cycling stability and fast reaction kinetics. The process of ion–solvent complex co-intercalation into host materials can be described by eqn (1):[35]

$$n\mathrm{A} + x\mathrm{e}^- + \mathrm{M}^{x+} + y\mathrm{solvent} \rightleftharpoons \mathrm{M}^{x+}(\mathrm{solvent})_y\mathrm{A}_n^{x-} \quad (1)$$

where A and M represent the host material and alkali/alkaline-earth metal, respectively, and n, x, and y are the number of host materials, electrons, and solvents, respectively. The reversible ion–solvent complexes intercalate/deintercalate into/from the host materials during the cycling process. To date, the ion–solvent co-intercalation phenomenon has been extensively investigated in various nonaqueous rechargeable batteries (including LIBs, sodium-ion batteries (SIBs), potassium-ion batteries (PIBs), magnesium-ion batteries (MIBs), and calcium-ion batteries (CIBs)).[36–40] To the best of our knowledge, however, less attention has been paid to summarizing the ion–solvent co-intercalation reactions in rechargeable battery systems.[41] Therefore, a comprehensive summary of alkali and alkaline-earth metal ion–solvent co-intercalation reactions in nonaqueous rechargeable batteries is very significant.

In this review, we first introduce the host materials and solvents for the reversible ion–solvent co-intercalation reaction in nonaqueous rechargeable batteries. Then, we discuss the recent progress on alkali and alkaline-earth metal ion–solvent co-intercalation reactions in nonaqueous rechargeable batteries, including LIBs, SIBs, PIBs, MIBs, and CIBs. Finally, future perspectives on the ion–solvent co-intercalation phenomenon in rechargeable batteries are also proposed.

2. The host materials and solvents for the reversible ion–solvent co-intercalation reaction

To date, the ion–solvent co-intercalation reaction has been investigated in various nonaqueous rechargeable batteries.[42]

Shuo Zhao obtained his M.S. degree from Nankai University in 2021, under the supervision of Prof. Shulei Chou and Prof. Fujun Li. His research interests focus on computational material science and battery materials.

Shu-Lei Chou is a Professor and the founding director of Institute for Carbon Neutralization, College of Chemistry and Materials Engineering, Wenzhou University. He obtained his Bachelor's degree (1999) and Master's degree (2004) from Nankai University, China. He received his PhD from the University of Wollongong in 2010. His research focuses on energy storage materials for battery applications, especially on novel composite materials, new binders, and new electrolytes for Li/Na batteries.

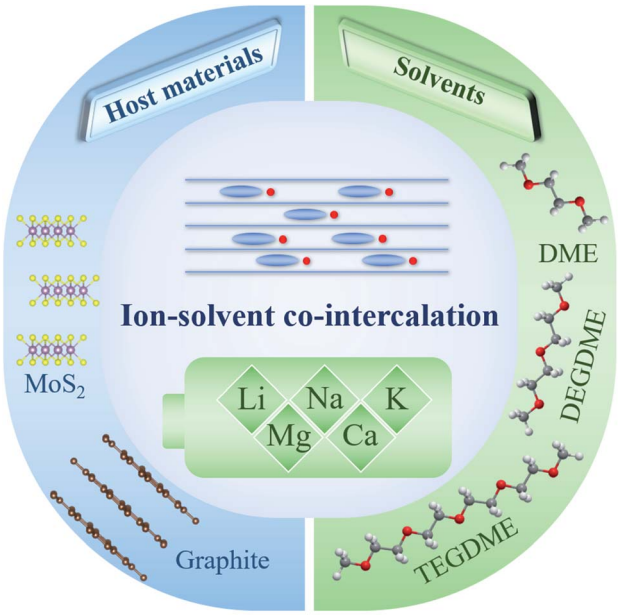

Fig. 1 The commonly used host materials and solvents for reversible ion–solvent co-intercalation reactions in various nonaqueous rechargeable batteries.

However, only a few host materials and solvents can realize reversible ion–solvent co-intercalation. Fig. 1 shows the commonly used host materials and solvents for the ion–solvent co-intercalation reaction in nonaqueous rechargeable batteries, including LIBs, SIBs, PIBs, MIBs and CIBs.

2.1 Host materials

Host materials play an important role in ion–solvent co-intercalation in rechargeable batteries. Graphite is the most extensively used host material for ion–solvent co-intercalation.[43] To date, it has been applied for various nonaqueous rechargeable batteries (including LIBs, SIBs, PIBs, MIBs and CIBs).[44] In general, graphite with the ion–solvent co-intercalation reaction mechanism exhibits superior rate performance and cycling stability. In addition to graphite, the layered sulfide MoS_2 is also demonstrated as a host material for ion–solvent co-intercalation in LIBs and MIBs.[39,45,46] The solvated ion co-intercalation into MoS_2 shows ultrafast kinetics. Recently, the reversible Li^+-solvent co-intercalation in few-layered $Ti_3C_2T_x$ MXenes was observed by Placke *et al.*[47]

2.2 Solvents

In addition to host materials, the solvent is another key component in ion–solvent co-intercalation reactions. Linear ethers (including dimethoxyethane (DME), diethylene glycol dimethyl ether (DEGDME) and tetraethylene glycol dimethyl ether (TEGDME)) are the most commonly used solvents in ion–solvent co-intercalation systems.[48,49] In addition, some other solvents (such as triethylene glycol dimethyl ether, pentaglyme, poly(ethylene glycol) dimethyl ether, crown ethers, and dimethylacetamide) can realize reversible solvated ion co-intercalation into host materials.[40,50,51]

3. The ion–solvent co-intercalation phenomenon in various rechargeable batteries

3.1 Lithium-ion batteries

Graphite is a commonly used anode material in commercial LIBs, and it can also be used as a host material for the Li^+-solvent co-intercalation reaction.[18,52] However, the earlier reported ion–solvent co-intercalation reactions are not reversible, which can be ascribed to graphite exfoliation.[53,54] Thus, most research has focused on suppressing the Li^+-solvent co-intercalation in graphite.[55,56] The reversible Li^+-solvent co-intercalation into graphite in ether-based electrolyte was demonstrated by Adelhelm's group.[52] Subsequently, Kim *et al.* systematically investigated the Li^+-solvent co-intercalation into graphite in ether-based electrolyte.[57] They found that the reversible Li^+-solvent co-intercalation in graphite can be realized by appropriate solvent selection. The chemical compatibility of the $[Li\text{-solvent}]^+$ complex and graphite largely affects the reversibility of the co-intercalation reaction. They also demonstrated that the poor electrochemical performance of graphite is caused by the side reaction of Li metal. As shown in Fig. 2a, the graphite electrode with the co-intercalation mechanism shows better rate performance than conventional Li^+ intercalation. The superior rate performance can be attributed to the absence of a desolvation process, negligible solid electrolyte interphase (SEI) layer (Fig. 2b) and fast kinetics. This work indicated that the reversible Li^+-solvent co-intercalation in graphite is beneficial to achieve high-power-density LIBs. In addition, the potential for practical application was demonstrated by the $LiFePO_4$//graphite full cell, which shows superior cycling stability (capacity retention of ~80% after 200 cycles). Recently, an abnormal overcharging phenomenon was observed when using lithium bis-trifluoromethane sulfonimide (LiTFSI) as a lithium salt to investigate the co-intercalation of Li–ether solvent into graphite.[58] Lee and co-workers found that the abnormal overcharging was attributable to the shuttling mechanism, which was caused by the reduction of $TFSI^-$ anion. In addition, they proposed an effective strategy (adding $LiNO_3$ to the electrolyte) to suppress the abnormal overcharging.

MoS_2 is another host material which can realize reversible Li^+-solvent co-intercalation in ether-based electrolytes.[46] As shown in Fig. 2c, MoS_2 shows superior cyclic stability in the voltage window of 1.0–3.0 V because only the co-intercalation reaction occurred. The Li^+-solvent co-intercalation reaction mechanism was demonstrated by investigating the mass variation of the electrodes during the discharge process and Fourier transform infrared spectroscopy (FTIR) spectra of the electrolyte and electrodes at different states. In addition, they found that the lithium storage mechanism is closely affected by the solvent species, which is similar to that of the Li–graphite system. The reversible co-intercalation reaction occurred when using linear ether as the solvent. The $[Li\text{–solvent}]^+$-intercalated MoS_2

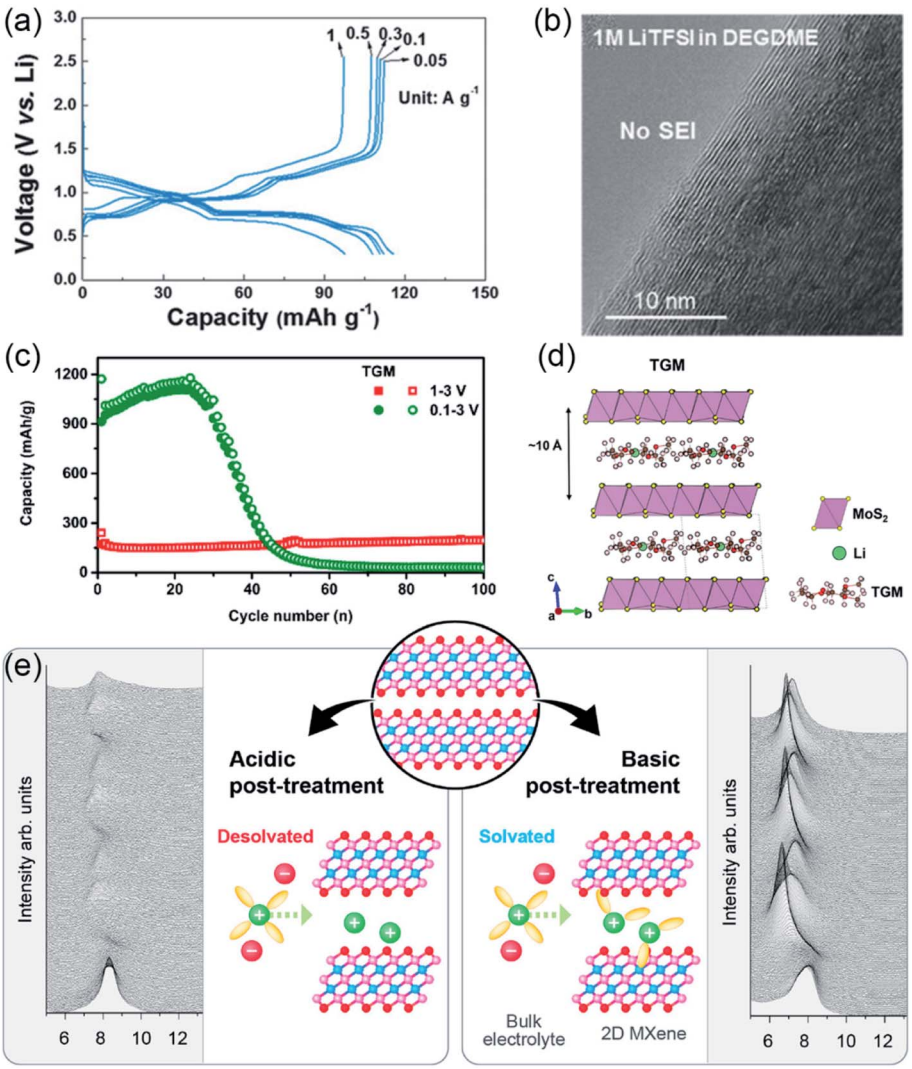

Fig. 2 Ion–solvent co-intercalation phenomenon in LIBs. (a) The rate performance of the graphite electrode in 1 M lithium bis(trifluoromethanesulfonyl)imid (LiTFSI) DEGDME electrolyte. (b) Transmission electron microscopy (TEM) images of graphite cycled in 1 M LiTFSI DEGDME. (a and b) Reproduced with permission.[57] Copyright 2017, Wiley-VCH. (c) The cycling performance of MoS_2 in 1 M LiTFSI TEGDME. (d) The structure of $[Li–solvent]^+$ intercalated in MoS_2. (c and d) Reproduced with permission.[46] Copyright 2017, American Chemical Society. (e) Schematic illustrating the lithium storage mechanism of the acidic and basic post-treatment of $Ti_3C_2T_x$ MXenes, which was investigated by *in situ* XRD. Reproduced with permission.[47] Copyright 2021, American Chemical Society.

structure was first proposed by theoretical calculations (Fig. 2d). MoS_2 with the co-intercalation mechanism exhibited superior cyclic stability (193.1 mA h g^{-1} after 2000 cycles) and good rate performance (77 mA h g^{-1} at 50 A g^{-1}). This work suggested that MoS_2 is a promising candidate electrode material for fast-charging LIBs.

In addition to graphite and MoS_2, the Li^+-solvent co-intercalation phenomenon was observed in few-layered $Ti_3C_2T_x$ MXenes.[47] As shown in Fig. 2e, Li^+-solvent co-intercalation occurred when using basic post-treatment $Ti_3C_2T_x$ as the anode, which was demonstrated by *in situ* XRD. Interestingly, a reversible ion intercalation/deintercalation reaction was observed for the acidic post-treatment samples. Based on the above results, Placke *et al.* proposed a possible explanation that polar solvents can intercalate more easily due to the preintercalated cations formed during the basic post-treatment. However, this hypothesis needs to be further verified by providing more evidence.

3.2 Sodium-ion batteries

Unlike LIBs, the binary graphite intercalation compounds (GICs) of sodium cannot form electrochemically in SIBs.[59,60] Therefore, graphite was not considered as an anode material for SIBs until Adelhelm's group found the unique Na^+–solvent co-intercalation mechanism in ether-based electrolyte.[35] Highly reversible sodium storage in graphite is realized by the unique reaction mechanism. The graphite electrode shows low overpotential, small irreversible capacity, superior cycling stability and good rate performance (Fig. 3a–c). It is worth noting that graphite electrodes show better rate performance for Na^+–

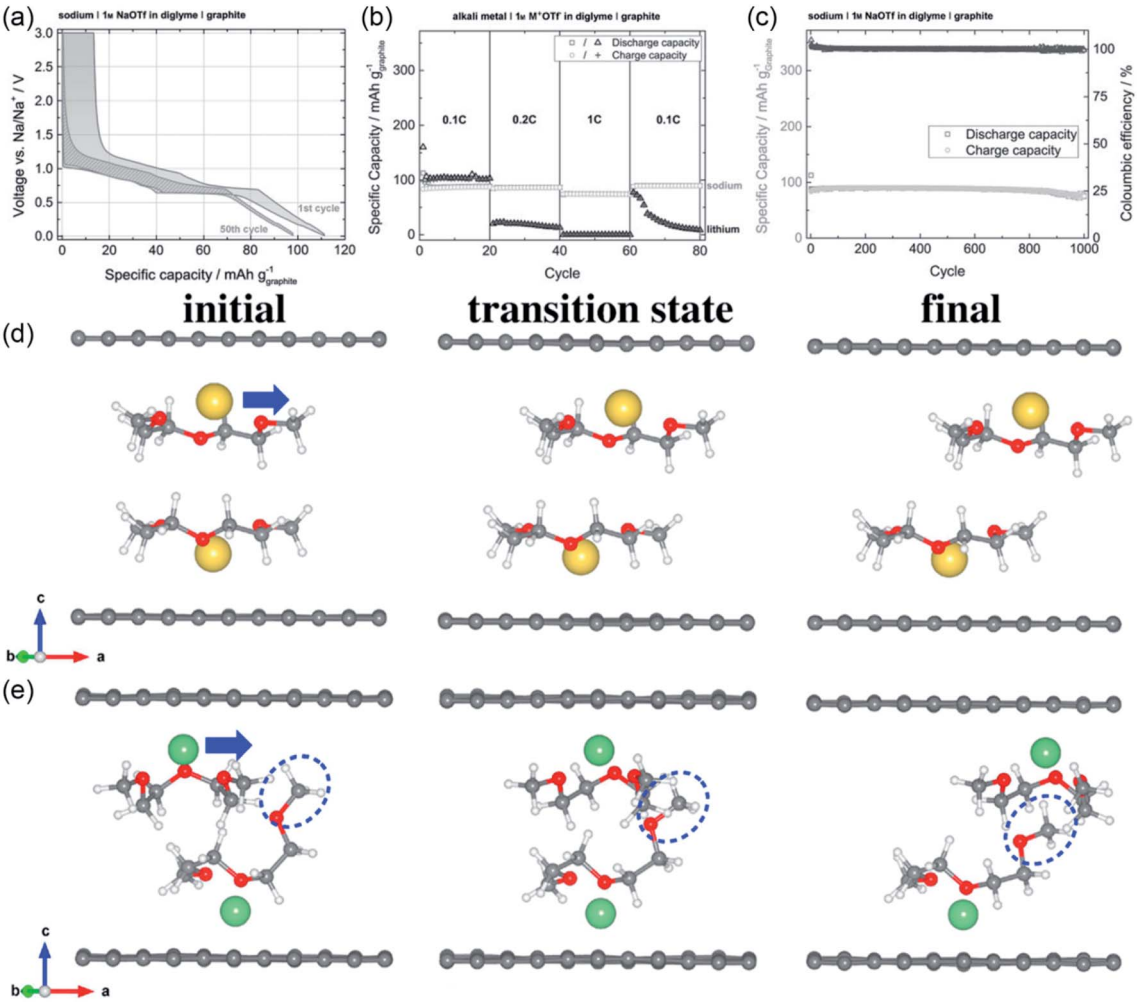

Fig. 3 The ion–solvent co-intercalation phenomenon in SIBs. (a) Charge/discharge curves, (b) rate performance and (c) cycling performance of graphite in diglyme-based electrolyte. (a–c) Reproduced with permission.[35] Copyright 2014, Wiley-VCH. The structures of (d) Na^+–diglyme and (e) Li^+–diglyme codiffusions in graphite. (d and e) Reproduced with permission.[61] Copyright 2017, Elsevier.

solvent co-intercalation than for Li^+-solvent co-intercalation (Fig. 3c). To better understand this phenomenon, the diffusion of ion–solvent complexes in graphite was investigated by theoretical calculations.[61] As shown in Fig. 3d, the Na^+–diglyme complexes can diffuse rapidly in graphite due to the flat diglyme molecules. The diffusion of the Li^+–diglyme complexes is slow in graphite because of steric hindrance caused by bent diglyme molecules (Fig. 3e). The Li^+–diglyme complexes diffusivity (1.2×10^{-13} cm^2 s^{-1}) is obviously slower than the diffusivity of the Na^+–diglyme complexes (1.1×10^{-8} cm^2 s^{-1}). Therefore, the Na^+–diglyme co-intercalation in graphite shows better rate performance. In addition, the reason for the superior cyclic stability of the graphite electrode was also investigated. The result reveals that the diglyme-graphene vdW interaction is beneficial for improving the interlayer coupling strength in Na^+–diglyme co-intercalated graphite. Therefore, the Na^+–diglyme co-intercalated shows stable mechanical integrity, which results in superior cycling stability.

Moreover, understanding the unique sodium storage mechanism is very important to develop graphite anodes for high-performance SIBs. Thus, the charge storage mechanism of Na^+–solvent co-intercalation in graphite was investigated by cyclic voltammetry (CV).[62] As shown in Fig. 4a, the electrochemical reaction occurred, combined with capacitive and intercalation reactions. The Na^+–solvent co-intercalation mechanism was demonstrated by *ex situ* X-ray photoelectron spectroscopy (XPS) and FTIR. The Na peaks in the Na 1s spectra were reversibly changed during charge/discharge processes, indicating reversible sodium storage in graphite (Fig. 4b). As shown in Fig. 4c, the peak of solvated Na^+ appeared after discharge, which revealed the Na^+–solvent complex was intercalated into graphite. All the results support the Na^+–solvent co-intercalation in graphite.

Subsequently, Kang's group further investigate the sodium storage mechanism by combining experiments and theoretical calculations.[63] The *in operando* synchrotron X-ray diffraction (XRD) was used to reveal the structural evolution of graphite electrodes during the charge/discharge process (Fig. 4d). The graphite electrode shows a typical staging structural evolution during the charge/discharge process, and a stage 1 GIC with a *c*

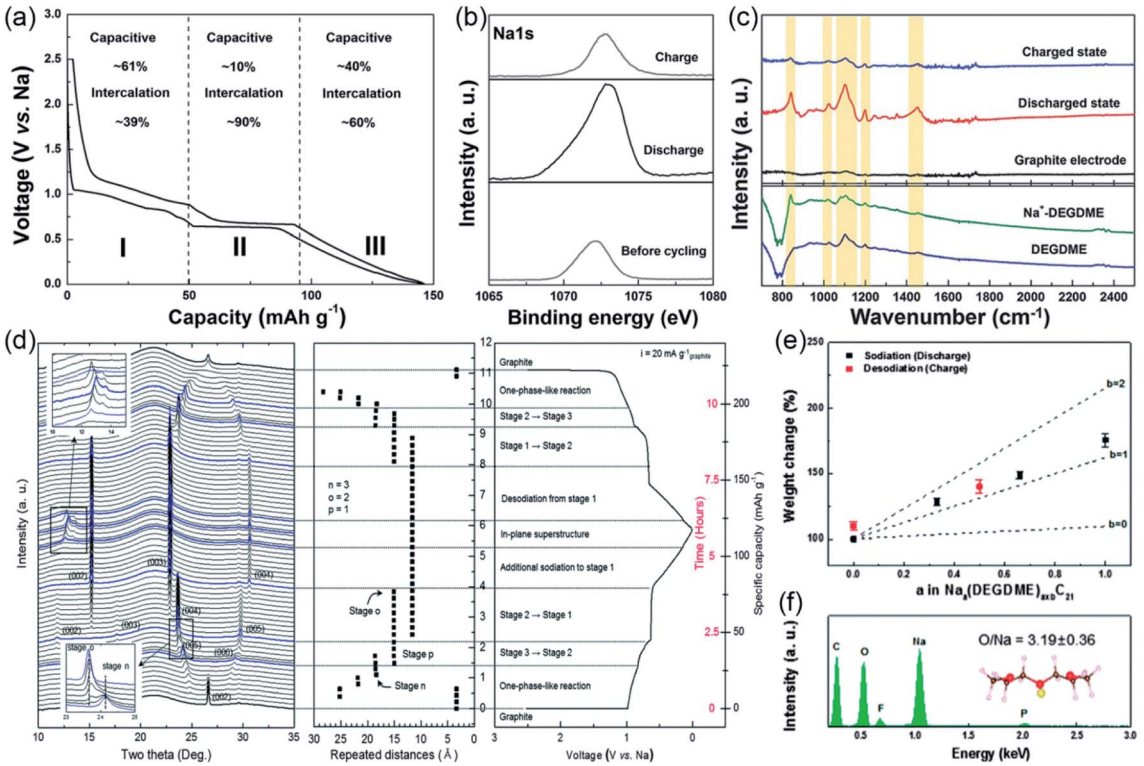

Fig. 4 Sodium storage mechanism. (a) Charge/discharge curves and charge storage mechanism of graphite electrode. (b) The XPS spectra of Na 1s. (c) FTIR spectra of the graphite electrode, solvent and electrolyte. (a–c) Reproduced with permission.[62] Copyright 2015, Wiley-VCH. The structures for (d) *in operando* synchrotron XRD of the graphite electrode. (e) Weight change of the graphite electrode during charge/discharge process. (f) Energy-dispersive X-ray spectroscopy of the graphite electrode in the discharge state. (d–f) Reproduced with permission.[63] Copyright 2015, Royal Society of Chemistry.

lattice parameter of 11.62 Å was formed after discharge. In addition, the number of intercalated solvent molecules per Na^+ in graphite is investigated by monitoring the weight change of the electrode during the charge/discharge process and the ratio of O/Na in the stage 1 GICs (Fig. 4e and f). The result reveals that one solvent molecule is intercalated into graphite with one Na^+. Based on the above experimental results, they further investigated the structure of Na–DEGDME–graphite GICs by theory calculations. They proposed a model with double stacking of the $[Na–DEGDME]^+$ complex. Recently, Stimming and co-workers visualized the phase transitions on the atomic scale by electrochemical scanning tunneling microscopy (EC-STM) for the first time.[64] The large lattice expansions were also observed by *in operando* EC-STM, which indicated that the Na^+–solvent co-intercalation mechanism has occurred.

It is worth noting that the unique reversible Na^+–solvent co-intercalation mechanism occurs only when using specific solvents (Fig. 5a).[65] Some different electrochemical behaviors (such as irreversible Na^+–solvent co-intercalation and electrochemical inactivity) are observed in the other solvents. To explain this phenomenon, the conditions for reversible Na^+–solvent co-intercalation were investigated by theoretical calculations. The solvation energy and the lowest unoccupied molecular orbital (LUMO) levels of the Na^+–solvent complexes were applied to estimate the thermodynamic stability of the Na^+–solvent complexes and the chemical stability of the Na^+–solvent complexes in graphite, respectively. These results indicated that reversible Na^+–solvent co-intercalation requires strong solvation of Na^+ and a high LUMO level of the $[Na–solvent]^+$ complexes in graphite (Fig. 5b).

It is well known that the SEI layer plays a key role in the electrochemical performance of electrode materials.[66] The effect of the SEI on the co-intercalation reaction was first investigated by Adelhelm's group.[52] They found that a pre-formed SEI can suppress solvent co-intercalation in the first two cycles. Although this result supports a (nearly) SEI-free surface, the nature of the SEI of co-intercalation reactions is still unclear. Subsequently, Maibach *et al.* investigated the surface layer evolution on graphite during the charge/discharge process by soft XPS.[67] A thin SEI layer (3–8 nm) was formed on the cycled electrodes, which did not suppress solvent co-intercalation. In addition, SEI formation on the graphite electrode was observed by STM and electrochemical quartz crystal microbalance.[64] However, Adelhelm's group proposed a different opinion.[68] An SEI-free graphite anode material was demonstrated by combined TEM analysis and electrochemical results. The seemingly conflicting findings are attributed to the difference in the stability of the ether-based electrolyte with different sodium salts.[69]

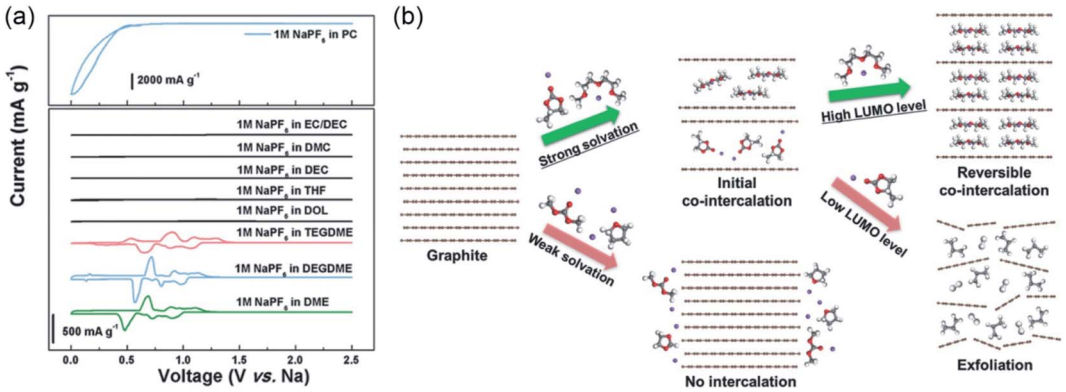

Fig. 5 The conditions for reversible Na^+–solvent co-intercalation into graphite. (a) CV curves of graphite electrodes in different electrolytes. (b) Schematic of the solvent dependency of Na–solvent co-intercalation behavior. Reproduced with permission.[65] Copyright 2017, Wiley-VCH.

Recently, Lu's group further investigated the reason for the superior stability of the SEI layer under the large volume changes of graphite anode.[70] The mechanical properties of the SEI were investigated by atomic force microscopy. The results demonstrated that the SEI possessed a high Young's modulus. In addition, XPS with depth sputtering was utilized to investigate the components of the SEI. The SEI showed a multilayer structure (the surface layer is dominated by organic compounds while the inorganic compounds are primarily distributed in the interior region). The organic components in the surface layer improve the adaptability to volume changes. The concentrated distribution of inorganic components in the inner layer results in a high Young's modulus. Therefore, the SEI maintains superior stability under the substantial volume changes during charge/discharge processes.

Although the mechanism of co-intercalation of graphite with Na^+–solvent exhibits superior electrochemical performance, the high redox potential inevitably lowers the energy density. Therefore, finding an effective strategy to tune the discharge voltage of graphite is very significant. The effect of solvent species on the discharge voltage was first investigated by Kang's group.[62] They found that the discharge voltage of graphite electrode increases with the increase of the chain length of the linear ether solvent. They attributed this phenomenon to the fact that solvent molecules with longer chain lengths are beneficial for forming more stable discharge products. However, the underlying reasons for this phenomenon are still unclear. Thus, they further investigated the phenomenon in a following work, where they found that the discharge voltage was closely related to the screening effect by the solvent molecules.[63] The solvent molecules with longer chains exhibit a stronger screening effect, which results in a more stable discharge product.

Recently, they demonstrated that the salt concentrations and operation temperatures can also affect the co-intercalation potentials of graphite electrodes.[51] As shown in Fig. 6a, a low discharge voltage of 0.43 V was achieved by adjusting the operation temperatures of batteries and the solvent species and salt concentrations of the electrolyte. Benefiting from the voltage tuning, a Na-ion full cell with $Na_{1.5}VPO_{4.8}F_{0.7}$ as the cathode and graphite as the anode showed a high discharge voltage of ~3.1 V (Fig. 6b). In addition, the full cell exhibited superior rate performance (~80% of the capacity retained at 4 A g^{-1}) and cycling stability (capacity retention of 93% after 1000 cycles), indicating that the Na ion full cell is a promising candidate for next-generation energy storage systems (Fig. 6c and d).

3.3 Potassium-ion batteries

Since Ji *et al.* reported the electrochemical potassium storage performance of graphite in 2015, graphite has attracted extensive attention as an anode material for PIBs.[71–73] However, the graphite electrode shows poor electrochemical performance in conventional ester-based electrolyte. Owing to the superior electrochemical performance of graphite electrodes in SIBs when using ether-based electrolyte, the electrochemical performance of K/graphite batteries in ether-based electrolyte was also investigated.[74–76] Pint's group first reported that the graphitic carbon electrode in PIBs can achieve superior electrochemical performance by using ether-based electrolyte (Fig. 7a).[38] The free-standing multi-layered graphene (MLG) foam electrode exhibits good rate performance (~80% capacity retention at 10 A g^{-1}, Fig. 7b) and excellent cycling stability (capacity retention of 95% over 1000 cycles). Similar to the SIBs system, a unique K^+–solvent co-intercalation mechanism was proposed. The sequential formation of stage 4, 3, 2 and 1 GIC was revealed by *in situ* Raman spectroscopy (Fig. 7c and d). In addition, the graphite electrode shows a higher discharge voltage in DEGDME-based electrolyte than in DME-based electrolyte. This phenomenon can be attributed to the difference of the screening effect of K^+ by the solvent molecules.

To better understand the co-intercalation mechanism, our group used *in situ* XRD to reveal the structural evolution during the charge/discharge processes.[77] As shown in Fig. 7e, a highly reversible multiple staging reaction occurs. To determine the stage number of the GICs after discharge, the height expansion of the highly oriented pyrolytic graphite (HOPG) after full potassiation was studied. The height of the HOPG changed from 1.503 to 4.834 mm after it was fully potassiated. This result

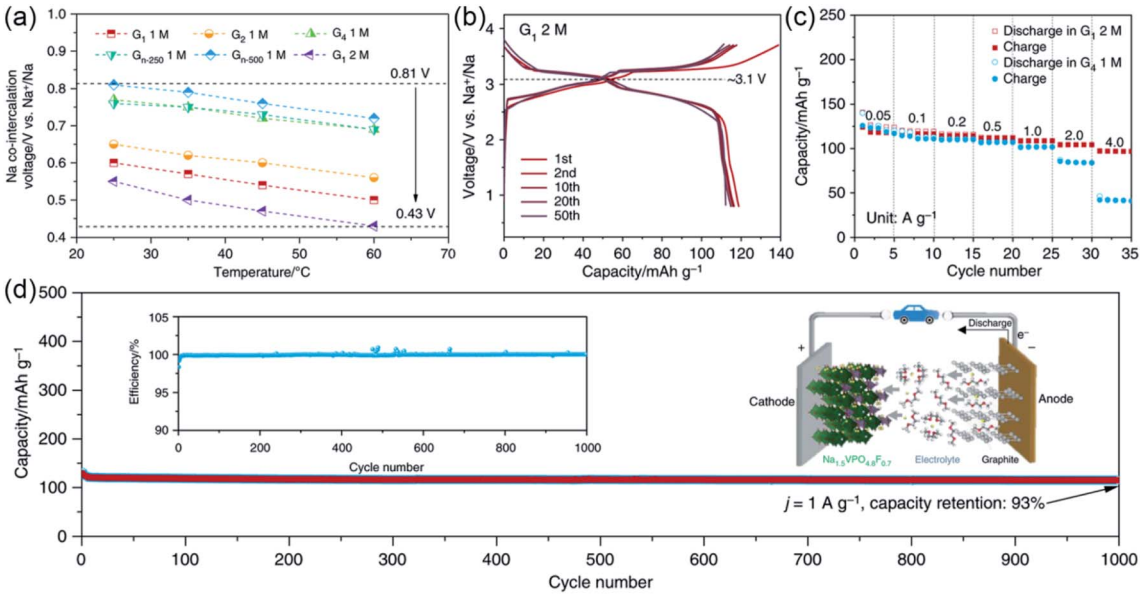

Fig. 6 Regulation of the co-intercalation potential. (a) Discharge voltages of graphite electrode at different temperatures in different electrolytes. (b) Charge/discharge curves of a Na-ion full cell. (c) Rate performance and (d) cycling performance of the Na-ion full cell. Reproduced with permission.[51] Copyright 2019, Nature Publishing Group.

indicated that a stage 1 GIC was formed after discharge. Subsequently, the number of solvent molecules intercalated with one K^+ was investigated by measuring the weight change of the graphite electrode during the discharge process. The weight change supported intercalation of one DEGDME molecule with one K^+. Then, the structure of the stage 1 GIC was further investigated by first-principles calculations. As shown in Fig. 7f, the structure composed of two $[K–DEGDME]^+$ complexes intercalated in graphite was proposed. In addition, the conditions for reversible K^+–solvent co-intercalation were investigated by combining experiments and theoretical calculations. The results reveal that the reversible K^+–solvent co-intercalation requires strong solvation of K^+ and a high LUMO energy level of the $[K–solvent]^+$ complex.

The intercalation chemistry of various solvated alkali ions (M = Li, Na and K) in graphite was comparative investigated by Kang's group.[78] They found that the average voltage of the graphite electrodes increases with the ion radius (Fig. 7g). The reason for this phenomenon was investigated by experiments and theoretical calculations. The XRD analysis reveals that the interlayer distance increases with the cation size. The theoretical calculations demonstrate that the repulsion between negatively charged graphene layers in the discharged state is the key reason for the different alkali ion storage voltages (Fig. 7h and i). The repulsion between negatively charged graphene layers in the discharged state is reduced as the interlayer distance increases, which results in improved alkali ion storage voltage.

Recently, our group assembled a potassium-ion full cell based on the K^+–solvent co-intercalation reaction by using $K_{1.84}Ni[Fe(CN)_6]_{0.88}\cdot 0.49H_2O$ (KNiHCF) as the cathode, 1 M KPF_6 DEGDME as the electrolyte and graphite as the anode.[79] The KNiHCF//graphite full cell shows a high discharge voltage of ~2.84 V, high power density of 6889 W kg^{-1} and superior cycling performance (capacity retention of 87.1% after 500 cycles), which demonstrated that the potassium-ion full cell based on the K^+–solvent co-intercalation reaction mechanism is a promising candidate for practical application.

3.4 Magnesium-ion batteries

Similar to Na^+, Mg^{2+} cannot reversibly intercalate into graphite in conventional electrolyte systems.[80] In 1988, Maeda *et al.* demonstrated that the Mg^{2+}–solvent can undergo electrochemical insertion into HOPG in dimethylsulfoxide-based electrolyte.[81] Subsequently, Schmuck's group also reported reversible Mg^{2+}–solvent co-intercalation into graphite in 0.5 M $Mg(TFSI)_2$/*N*,*N*-dimethyformamide (DMF).[82] However, the graphite electrode shows a low specific capacity, which hinders its practical application (Fig. 8a). Inspired by the superior electrochemical performance of Na^+–solvent co-intercalation into graphite in ether-based electrolyte, Lee's group investigated the Mg^{2+} storage behaviors of graphite in DME and DEGDME-based electrolyte (Fig. 8b).[83] The results reveal that the solvated Mg^{2+} can reversibly insert into graphite with a high capacity of 180 mA h g^{-1} (Fig. 8c). The co-intercalation mechanism was demonstrated by XRD and FTIR.

In addition to graphite, MoS_2 can reversibly store solvated Mg^{2+}.[39] The $[Mg(DME)_3]^{2+}$ ions are reversibly inserted into MoS_2@C porous nanorods (MoS_2@C-PNR) with fast kinetics. Therefore, the MoS_2@C-PNR electrode exhibits high discharge capacity, good cycling stability and superior rate performance (Fig. 8d–f). In addition, the Mg storage mechanism was investigated by XRD, XPS, and TEM. The possible electrochemical reactions are proposed as follows:

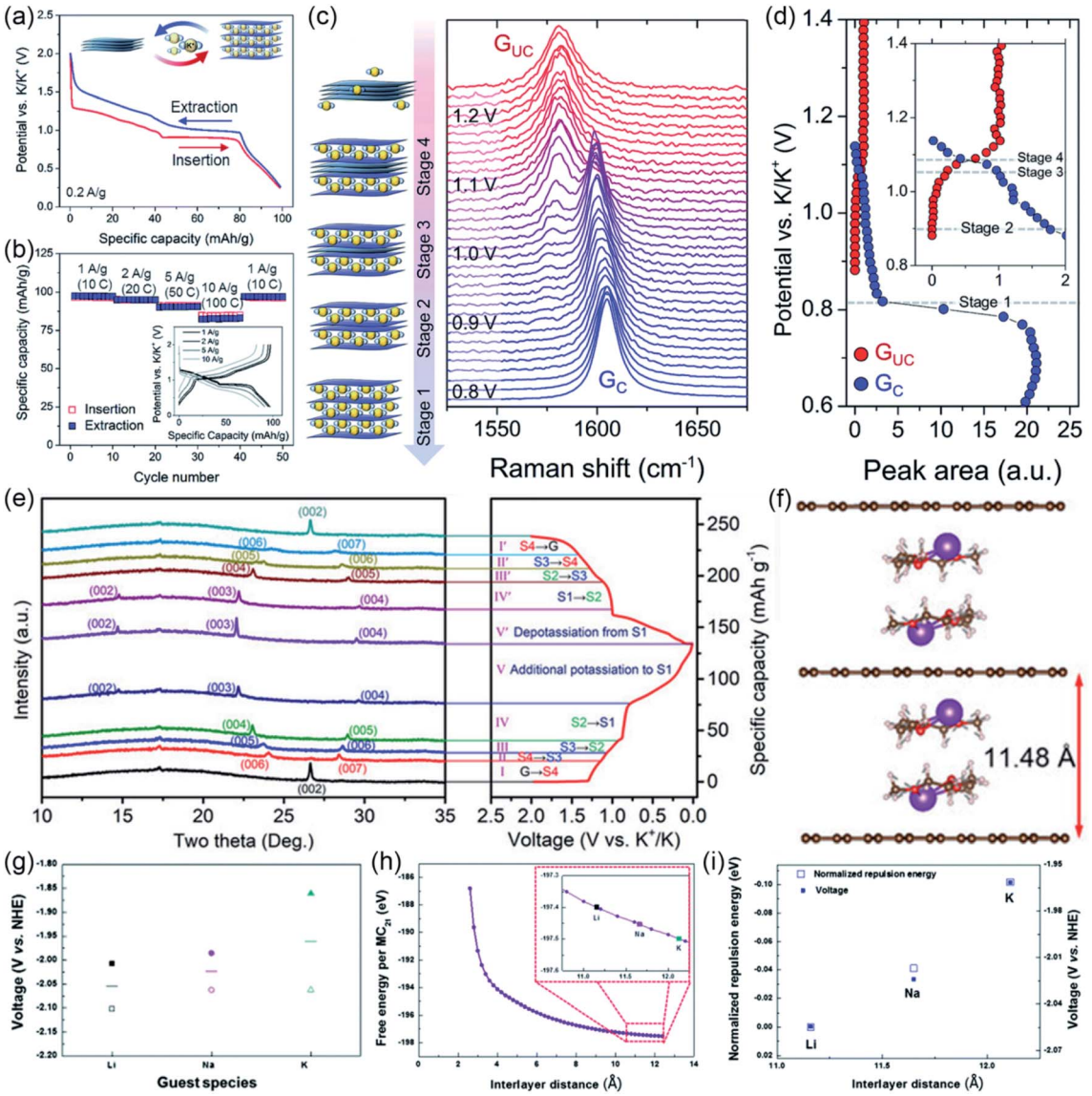

Fig. 7 Ion–solvent co-intercalation phenomenon in PIBs. (a) Charge/discharge curves and (b) rate performance (inset: corresponding charge/discharge curves) of MLG foam in ether-based electrolyte. (c) *In situ* Raman spectrum of MLG foam. (d) The relative peak areas of the two G peaks. (a–d) Reproduced with permission.[38] Copyright 2016, Royal Society of Chemistry. (e) The partial XRD patterns of characteristic stages of the GICs and the corresponding charge/discharge curves. (Note: S1, stage 1; S2, stage 2; S3, stage 3; S4, stage 4; G, graphite.) (f) The structure of two $[K–DEGDME]^+$ complexes intercalated in graphite (red, gray, white and purple balls represent O, C, H and K atoms, respectively). (e and f) Reproduced with permission.[77] Copyright 2020, Wiley-VCH. (g) The average voltage of graphite electrode in different battery systems (line: average voltage, filled symbols: charge voltage, empty symbols: discharge voltage). (h) Free energy of the negatively charged graphite framework (one charge injected in 21 C atom) as a function of interlayer distance (inset: magnification of the red square). (i) Voltage and normalized repulsion energy as a function of interlayer distance (filled squares: voltage, open squares: normalized repulsion energy). (g–i) Reproduced with permission.[78] Copyright 2016, Royal Society of Chemistry.

$$MoS_2\ (2H) + x[Mg(DME)_n]^{2+} + 2xe^- \rightarrow [Mg(DME)_n]_xMoS_2\ (1T) \quad (2)$$

$$[Mg(DME)_n]_xMoS_2\ (1T) \leftrightarrow (DME)_yMoS_2\ (2H) + x[Mg(DME)_n]^{2+} + 2xe^- \quad (3)$$

3.5 Calcium-ion batteries

Recently, reversible Ca^{2+}–solvent co-intercalation into graphite was reported by Pyo's group (Fig. 9a).[84] They designed graphite/activated carbon batteries to avoid the influence of the Ca surface passivation. They demonstrated that the reversible Ca^{2+}–solvent co-intercalation can occur in 1 M $Ca(TFSI)_2$ G4 electrolyte due to the strong solvation of Ca^{2+}. The co-intercalation mechanism was investigated by energy dispersive X-ray (EDX) images, XPS, Raman spectroscopy, *in operando*

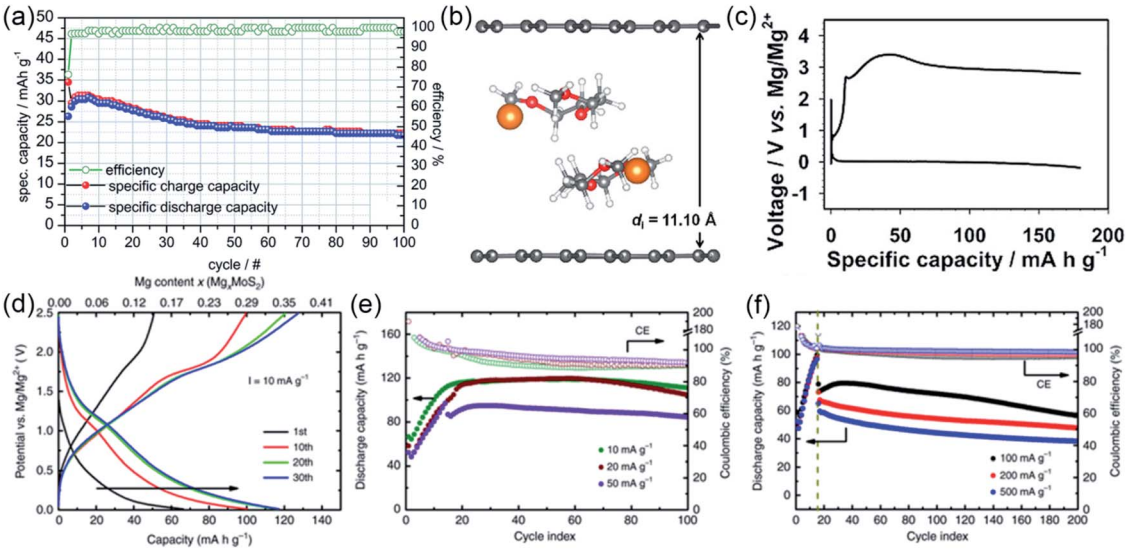

Fig. 8 Ion–solvent co-intercalation phenomenon in MIBs. (a) Cycling performance of natural graphite in 0.5 M $Mg(TFSI)_2$/DMF. Reproduced with permission.[82] Copyright 2017, The Royal Society of Chemistry. (b) The structure of Mg^{2+}–DEGDME co-intercalated graphite. (c) Charge/discharge curves of graphite electrode in 0.3 M $Mg(TFSI)_2$ DME/DEGDME electrolyte. (b and c) Reproduced with permission.[83] Copyright 2018, American Chemical Society. (d) Charge/discharge profiles of MoS_2@C-PNR electrode. (e and f) Cycling performance of MoS_2@C-PNR electrode at different current densities. (d–f) Reproduced with permission.[39] Copyright 2018, Nature Publishing Group.

synchrotron XRD patterns and density functional theory calculations. In addition, they fabricated a rocking-chair type calcium-ion battery (Ca^{2+}-loaded graphite/perylene-3,4,9,10-tetracarboxylic dianhydride), which showed superior electrochemical performance with a reversible voltage of about 1.6 V (Fig. 9b and c). At about the same time, Kang and co-workers also found the ion–solvent co-intercalation phenomenon in CIBs with dimethylacetamide (DMAc)-based electrolyte.[40] The co-intercalation mechanism was revealed by FTIR and ^{13}C nuclear magnetic resonance (NMR) spectroscopy. As shown in Fig. 9d, the ^{13}C-NMR spectra of the calciated graphite, DMAc-based electrolyte and DMAc solvent exhibited four peaks at similar positions, which indicated that the DMAc was co-intercalated with Ca^{2+} into graphite. To better understand the co-intercalation mechanism, they measured the weight change during the charge/discharge process to determine the number of DMAc molecules intercalated with one Ca^{2+} (Fig. 9e). The results indicated that four DMAc molecules intercalated with one Ca^{2+} during the charging process. Moreover, the structure of the $[Ca(DMAc)_4]^{2+}$ co-intercalated graphite was proposed by

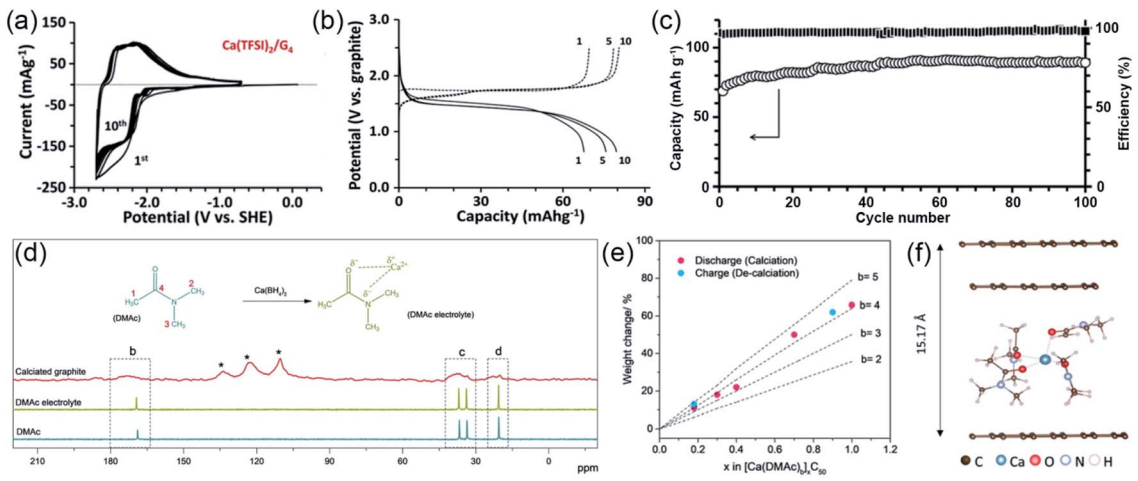

Fig. 9 Ion–solvent co-intercalation phenomenon in CIBs. (a) CVs of graphite electrode in 1 M $Ca(TFSI)_2$ G4 electrolyte. (b) The charge/discharge curves of a full cell. (c) The cycling performance of the full cell. (a–c) Reproduced with permission.[84] Copyright 2019, Wiley-VCH. (d) ^{13}C-NMR spectra of the calciated graphite, DMAc-based electrolyte and DMAc solvent. (e) Weight changes of graphite measured in various charge and discharge states. (f) The structure of the $[Ca(DMAc)_4]^{2+}$ co-intercalated graphite. (d–f) Reproduced with permission.[40] Copyright 2019, Wiley-VCH.

density functional theory calculations (Fig. 9f). Most recently, Pyo *et al.* constructed a Ca^{2+}-based dual-carbon battery by using 0.5 M [Ca:G4] Pyr14TFSI electrolyte.[85] During the charging process, the [Ca:G4] co-intercalated into graphite anode.

4. Conclusions and perspectives

The ion–solvent co-intercalation phenomenon has attracted extensive attention in nonaqueous rechargeable battery systems due to its fast kinetics. The fast kinetics is beneficial to improve the rate performance of electrode materials and thus realize fast-charging batteries. However, the ion–solvent co-intercalation reaction only occurs when using specific solvent species and host materials. In this review, we have summarized recent progress on the ion–solvent co-intercalation phenomenon in various battery systems, including LIBs, SIBs, PIBs, MIBs and CIBs. The Na^+–solvent co-intercalation in graphite is very significant because the naked Na^+ cannot intercalate into graphite. Therefore, the ion–solvent co-intercalation reaction in SIBs has been systematically and comprehensively investigated (such as the reason for the superior electrochemical performance, ion–solvent co-intercalation mechanism, conditions for reversible ion–solvent co-intercalation and strategies for adjusting the co-intercalation potential). However, to date, only graphite has been used as host material for the co-intercalation reaction. Thus, developing other high-performance host materials for the reversible Na^+–solvent co-intercalation is necessary. The ion–solvent co-intercalation reaction in other battery systems is still in its infancy. All of the methods for investigating the co-intercalation reaction mentioned in SIBs show great potential for other battery systems (including LIBs, PIBs, MIBs and CIBs). The electrochemical performance of the Li^+-solvent co-intercalation reaction in LIBs is poor, which needs further improvement. Among these monovalent ion batteries (including LIBs, SIBs and PIBs), PIBs show the highest average voltage for the co-intercalation reaction. Therefore, finding an effective strategy to reduce the co-intercalation potential is very meaningful. For MIBs, it is necessary to fabricate full cells to demonstrate the potential of the co-intercalation reaction for practical application. The Ca^{2+}–solvent co-intercalation reaction in graphite occurs in different solvent species. It is significant to investigate the conditions for reversible Ca^{2+}–solvent co-intercalation.

Although ion–solvent co-intercalation reactions have been extensively applied in various battery systems due to their unique advantages, there are still some challenges that must be addressed to achieve their practical application for fast-charging batteries (Fig. 10). First, the electrode materials with the ion–solvent co-intercalation reaction mechanism generally show high redox potential and low reversible capacity, which will reduce the energy density of the full cells. Second, the large volume change during the charge/discharge process will place a higher requirement on the manufacturing level of the battery and will be detrimental to its long-term stability. Third, the solvents participating in the reaction process could need more electrolyte, which would decrease the energy density of the full cells. Fourth, the mechanism of the ion–solvent co-intercalation reaction still remains a mystery. Therefore, it is very necessary to further investigate the ion–solvent co-intercalation reactions to promote their practical applications in fast-charging batteries.

In general, to meet the demand for high-performance fast-charging batteries, it is suggested that further research based on the ion–solvent co-intercalation reaction focus on the following aspects. First, to develop novel host materials, it is suggested to further investigate the requirements of host materials to realize reversible ion–solvent co-intercalation. Second, exploring the solvent with superior electrochemical stability for the ion–solvent co-intercalation reaction is very meaningful. Third, to achieve high energy density of full cells, finding effective strategies to reduce the redox potential and increase the reversible capacity of the ion–solvent co-intercalation reaction is necessary. Fourth, designing a unique cell structure to alleviate the volume change during the charge/discharge process is desirable. Fifth, more *in situ* techniques and theoretical calculations are suggested to be employed to thoroughly investigate the ion–solvent co-intercalation phenomenon in nonaqueous rechargeable battery systems. Finally, full cell fabrication and research are critical to verify the potential practical application of the ion–solvent co-intercalation reaction in fast-charging batteries.

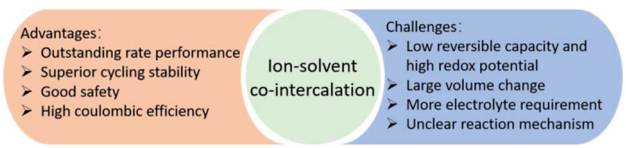

Fig. 10 The advantages and challenges of ion–solvent co-intercalation.

Author contributions

L. Li and S.-L. Chou proposed and designed the review. L. Li and Z. Hu prepared the draft. L. Li and S. Zhao conducted the literature research. S.-L. Chou finally revised the review.

Conflicts of interest

There are no conflicts to declare.

Acknowledgements

This work was supported by the National Key R&D Program of China (2017YFA0206700), the National Natural Science Foundation of China (21835004, 51971124 and 52171217), and 111 Project from the Ministry of Education of China (B12015).

References

1 *The International Energy Outlook 2020*, U.S. Energy Information Administration, 2020, https://www.eia.gov/outlooks/ieo/pdf/ieo2020.pdf.
2 P. E. Brockway, A. Owen, L. I. Brand-Correa and L. Hardt, *Nat. Energy*, 2019, **4**, 12–621.

3 M. D. Staples, R. Malina and S. R. H. Barrett, *Nat. Energy*, 2017, **2**, 16202.
4 P. C. Stern, K. B. Janda, M. A. Brown, L. Steg, E. L. Vine and L. Lutzenhiser, *Nat. Energy*, 2016, **1**, 16043.
5 S. Liu, L. Kang and S. C. Jun, *Adv. Mater.*, 2021, DOI: 10.1002/adma.202004689.
6 M. Zhou, P. Bai, X. Ji, J. Yang, C. Wang and Y. Xu, *Adv. Mater.*, 2021, **33**, 2003741.
7 B. Dunn, H. Kamath and J.-M. Tarascon, *Science*, 2011, **334**, 928–935.
8 L. Jiang, Y. Lu, C. Zhao, L. Liu, J. Zhang, Q. Zhang, X. Shen, J. Zhao, X. Yu, H. Li, X. Huang, L. Chen and Y.-S. Hu, *Nat. Energy*, 2019, **4**, 495–503.
9 Y. You, X.-L. Wu, Y.-X. Yin and Y.-G. Guo, *Energy Environ. Sci.*, 2014, **7**, 1643–1647.
10 L. Li, S. Zhao, Z. Hu, S.-L. Chou and J. Chen, *Chem. Sci.*, 2021, **12**, 2345–2356.
11 Y. Liang, Y. Jing, S. Gheytani, K.-Y. Lee, P. Liu, A. Facchetti and Y. Yao, *Nat. Mater.*, 2017, **16**, 841–848.
12 L. Fan, R. Ma, Q. Zhang, X. Jia and B. Lu, *Angew. Chem., Int. Ed.*, 2019, **58**, 10500–10505.
13 T. Hosaka, K. Kubota, A. S. Hameed and S. Komaba, *Chem. Rev.*, 2020, **120**, 6358–6466.
14 P. G. Bruce, S. A. Freunberger, L. J. Hardwick and J. M. Tarascon, *Nat. Mater.*, 2012, **11**, 19–29.
15 M. Ko, S. Chae, J. Ma, N. Kim, H.-W. Lee, Y. Cui and J. Cho, *Nat. Energy*, 2016, **1**, 16113.
16 W. Guo, Y.-X. Yin, S. Xin, Y.-G. Guo and L.-J. Wan, *Energy Environ. Sci.*, 2012, **5**, 5221–5225.
17 L. Zhang, X. Hu, Y. Wu, Y. Cao, C. Lin, C. Dong, G. Li, F. Xu, S. Zhang and K. Zhang, *Mater. Today Energy*, 2021, **21**, 100756.
18 M. Li, J. Lu, Z. Chen and K. Amine, *Adv. Mater.*, 2018, **30**, 1800561.
19 Z. Hou, X. Zhang, H. Ao, M. Liu, Y. Zhu and Y. Qian, *Mater. Today Energy*, 2019, **14**, 100337.
20 Y. Hou, X. Li, W. Liu, H. Kou, H. M. K. Sari, X. Song, J. Li, S. Dou, X. Liu, S. Deng, D. Li and X. Sun, *Mater. Today Energy*, 2019, **14**, 100353.
21 Z. Hu, Q. Liu, W. Lai, Q. Gu, L. Li, M. Chen, W. Wang, S.-L. Chou, Y. Liu and S. X. Dou, *Adv. Energy Mater.*, 2020, **10**, 1903542.
22 L. Li, Z. Hu, Y. Lu, S. Zhao, Q. Zhang, Q. Liu, Z. Yan and S.-L. Chou, *J. Energy Chem.*, 2021, DOI: 10.1016/j.jechem.2021.02.009.
23 L. Li, Y. Lu, Q. Zhang, S. Zhao, Z. Hu and S.-L. Chou, *Small*, 2021, **17**, 1902767.
24 D. Wang, X. Gao, Y. Chen, L. Jin, C. Kuss and P. G. Bruce, *Nat. Mater.*, 2018, **17**, 16–20.
25 M.-C. Lin, M. Gong, B. Lu, Y. Wu, D.-Y. Wang, M. Guan, M. Angell, C. Chen, J. Yang, B.-J. Hwang and H. Dai, *Nature*, 2015, **520**, 325–328.
26 Q. Zhang, Y. Ma, Y. Lu, L. Li, F. Wan, K. Zhang and J. Chen, *Nat. Commun.*, 2020, **11**, 4463.
27 Y. Liu, Y. Zhu and Y. Cui, *Nat. Energy*, 2019, **4**, 540–550.
28 B. Babu, P. Simon and A. Balducci, *Adv. Energy Mater.*, 2020, **10**, 2001128.
29 K. J. Griffith, Y. Harada, S. Egusa, R. M. Ribas, R. S. Monteiro, R. B. Von Dreele, A. K. Cheetham, R. J. Cava, C. P. Grey and J. B. Goodenough, *Chem. Mater.*, 2020, **33**, 4–18.
30 W. Cai, Y. X. Yao, G. L. Zhu, C. Yan, L. L. Jiang, C. He, J. Q. Huang and Q. Zhang, *Chem. Soc. Rev.*, 2020, **49**, 3806–3833.
31 H. Jin, S. Xin, C. Chuang, W. Li, H. Wang, J. Zhu, H. Xie, T. Zhang, Y. Wan, Z. Qi, W. Yan, Y.-R. Lu, T.-R. Chan, X. Wu, J. B. Goodenough, H. Ji and X. Duan, *Science*, 2020, **370**, 192–197.
32 Z. Hu, Z. Tai, Q. Liu, S.-W. Wang, H. Jin, S. Wang, W. Lai, M. Chen, L. Li, L. Chen, Z. Tao and S.-L. Chou, *Adv. Energy Mater.*, 2019, **9**, 1803210.
33 S. Liu, J. Mao, L. Zhang, W. K. Pang, A. Du and Z. Guo, *Adv. Mater.*, 2020, **33**, 2006313.
34 Z. Sun, Y. Liu, W. Ye, J. Zhang and C. Yuan, *Angew. Chem., Int. Ed.*, 2021, **60**, 7180–7187.
35 B. Jache and P. Adelhelm, *Angew. Chem., Int. Ed.*, 2014, **53**, 10169–10173.
36 S. Maruyama, T. Fukutsuka, K. Miyazaki and T. Abe, *Electrochemistry*, 2020, **88**, 79–82.
37 Z. Zhu, F. Cheng, Z. Hu, Z. Niu and J. Chen, *J. Power Sources*, 2015, **293**, 626–634.
38 A. P. Cohn, N. Muralidharan, R. Carter, K. Share, L. Oakes and C. L. Pint, *J. Mater. Chem. A*, 2016, **4**, 14954–14959.
39 Z. Li, X. Mu, Z. Zhao-Karger, T. Diemant, R. J. Behm, C. Kubel and M. Fichtner, *Nat. Commun.*, 2018, **9**, 5115.
40 J. Park, Z. L. Xu, G. Yoon, S. K. Park, J. Wang, H. Hyun, H. Park, J. Lim, Y. J. Ko, Y. S. Yun and K. Kang, *Adv. Mater.*, 2020, **32**, 1904411.
41 J. Park, Z.-L. Xu and K. Kang, *Front. Chem.*, 2020, **8**, 432.
42 Y. Li, Y. Lu, P. Adelhelm, M.-M. Titirici and Y.-S. Hu, *Chem. Soc. Rev.*, 2019, **48**, 4655–4687.
43 Z.-L. Xu, J. Park, C. Yoon, H. Kim and K. Kang, *Small Methods*, 2019, **3**, 1800227.
44 P. Han, X. Han, J. Yao, L. Zhang, X. Cao, C. Huang and G. Cui, *J. Power Sources*, 2015, **297**, 457–463.
45 Q. Yun, L. Li, Z. Hu, Q. Lu, B. Chen and H. Zhang, *Adv. Mater.*, 2020, **32**, 1903826.
46 K. Zhang, G. Yoon, J. Zhang, M. Park, J. Yang, K. Kang and Y.-M. Kang, *ACS Appl. Energy Mater.*, 2019, **2**, 3726–3735.
47 P. Barmann, R. Nolle, V. Siozios, M. Ruttert, O. Guillon, M. Winter, J. Gonzalez-Julian and T. Placke, *ACS Nano*, 2021, **15**, 3295–3308.
48 A. P. Cohn, K. Share, R. Carter, L. Oakes and C. L. Pint, *Nano Lett.*, 2016, **16**, 543–548.
49 N. Karimi, A. Varzi and S. A. Passerini, *Electrochim. Acta*, 2019, **304**, 474–486.
50 M. Goktas, B. Akduman, P. Huang, A. Balducci and P. Adelhelm, *J. Phys. Chem. C*, 2018, **122**, 26816–26824.
51 Z.-L. Xu, G. Yoon, K.-Y. Park, H. Park, O. Tamwattana, S. J. Kim, W. M. Seong and K. Kang, *Nat. Commun.*, 2019, **10**, 2598.
52 B. Jache, J. O. Binder, T. Abe and P. Adelhelm, *Phys. Chem. Chem. Phys.*, 2016, **18**, 14299–14316.
53 G. C. Chung, H. J. Kim, S. I. Yu, S. H. Jun, J. W. Choi and M. H. Kim, *J. Electrochem. Soc.*, 2000, **147**, 4391–4398.

54 S. Maruyama, T. Fukutsuka, K. Miyazaki and T. Abe, *Electrochim. Acta*, 2018, **265**, 41–46.
55 J. Gao, H. P. Zhang, L. J. Fu, T. Zhang, Y. P. Wu, T. Takamura, H. Q. Wu and R. Holze, *Electrochim. Acta*, 2007, **52**, 5417–5421.
56 Y. Yamada, K. Usui, C. H. Chiang, K. Kikuchi, K. Furukawa and A. Yamada, *ACS Appl. Mater. Interfaces*, 2014, **6**, 10892–10899.
57 H. Kim, K. Lim, G. Yoon, J.-H. Park, K. Ku, H.-D. Lim, Y.-E. Sung and K. Kang, *Adv. Energy Mater.*, 2017, **7**, 1700418.
58 C. Y. Kim, G. H. Lee, H. A. So, K. H. Shin and Y. J. Lee, *ACS Appl. Mater. Interfaces*, 2020, **12**, 49541–49548.
59 K. Gotoh, H. Maruyama, T. Miyatou, M. Mizuno, K. Urita and H. Ishida, *J. Phys. Chem. C*, 2016, **120**, 28152–28156.
60 M. Liu, L. Xing, K. Xu, H. Zhou, J. Lan, C. Wang and W. Li, *Energy Storage Mater.*, 2020, **26**, 32–39.
61 S. C. Jung, Y.-J. Kang and Y.-K. Han, *Nano Energy*, 2017, **34**, 456–462.
62 H. Kim, J. Hong, Y.-U. Park, J. Kim, I. Hwang and K. Kang, *Adv. Funct. Mater.*, 2015, **25**, 534–541.
63 H. Kim, J. Hong, G. Yoon, H. Kim, K.-Y. Park, M.-S. Park, W.-S. Yoon and K. Kang, *Energy Environ. Sci.*, 2015, **8**, 2963–2969.
64 L. Seidl, N. Bucher, E. Chu, S. Hartung, S. Martens, O. Schneider and U. Stimming, *Energy Environ. Sci.*, 2017, **10**, 1631–1642.
65 G. Yoon, H. Kim, I. Park and K. Kang, *Adv. Energy Mater.*, 2017, **7**, 1601519.
66 H. Wang, D. Zhai and F. Kang, *Energy Environ. Sci.*, 2020, **13**, 4583–4608.
67 J. Maibach, F. Jeschull, D. Brandell, K. Edstrom and M. Valvo, *ACS Appl. Mater. Interfaces*, 2017, **9**, 12373–12381.
68 M. Goktas, C. Bolli, E. J. Berg, P. Novak, K. Pollok, F. Langenhorst, M. V. Roeder, O. Lenchuk, D. Mollenhauer and P. Adelhelm, *Adv. Energy Mater.*, 2018, **8**, 1702724.
69 M. Goktas, C. Bolli, J. Buchheim, E. J. Berg, P. Novak, F. Bonilla, T. Rojo, S. Komaba, K. Kubota and P. Adelhelm, *ACS Appl. Mater. Interfaces*, 2019, **11**, 32844–32855.
70 Z. Wang, H. Yang, Y. Liu, Y. Bai, G. Chen, Y. Li, X. Wang, H. Xu, C. Wu and J. Lu, *Small*, 2020, **16**, 2003268.
71 Z. Jian, W. Luo and X. Ji, *J. Am. Chem. Soc.*, 2015, **137**, 11566–11569.
72 J. Zhao, X. Zou, Y. Zhu, Y. Xu and C. Wang, *Adv. Funct. Mater.*, 2016, **26**, 8103–8110.
73 L. Fan, R. Ma, Q. Zhang, X. Jia and B. Lu, *Angew. Chem., Int. Ed.*, 2019, **58**, 10500–10505.
74 L. Wang, J. Yang, J. Li, T. Chen, S. Chen, Z. Wu, J. Qiu, B. Wang, P. Gao, X. Niu and H. Li, *J. Power Sources*, 2019, **409**, 24–30.
75 X. Liu, G. A. Elia, B. Qin, H. Zhang, P. Ruschhaupt, S. Fang, A. Varzi and S. Passerini, *ACS Energy Lett.*, 2019, **4**, 2675–2682.
76 K. Moyer, J. Donohue, N. Ramanna, A. P. Cohn, N. Muralidharan, J. Eaves and C. L. Pint, *Nanoscale*, 2018, **10**, 13335–13342.
77 L. Li, L. Liu, Z. Hu, Y. Lu, Q. Liu, S. Jin, Q. Zhang, S. Zhao and S.-L. Chou, *Angew. Chem., Int. Ed.*, 2020, **59**, 12917–12924.
78 H. Kim, G. Yoon, K. Lim and K. Kang, *Chem. Commun.*, 2016, **52**, 12618–12621.
79 L. Li, Z. Hu, Y. Lu, C. Wang, Q. Zhang, S. Zhao, J. Peng, K. Zhang, S.-L. Chou and J. Chen, *Angew. Chem., Int. Ed.*, 2021, **60**, 13050–13056.
80 P. Novak, R. Imhof and O. Haas, *Electrochim. Acta*, 1999, **45**, 351–367.
81 Y. Maeda, *Synth. Met.*, 1988, **24**, 267–270.
82 C. God, B. Bitschnau, K. Kapper, C. Lenardt, M. Schmuck, F. Mautner and S. Koller, *RSC Adv.*, 2017, **7**, 14168–14175.
83 D.-M. Kim, S. C. Jung, S. Ha, Y. Kim, Y. Park, J. H. Ryu, Y.-K. Han and K. T. Lee, *Chem. Mater.*, 2018, **30**, 3199–3203.
84 S. J. R. Prabakar, A. B. Ikhe, W. B. Park, K.-C. Chung, H. Park, K.-J. Kim, D. Ahn, J. S. Kwak, K.-S. Sohn and M. Pyo, *Adv. Sci.*, 2019, **6**, 1902129.
85 S. J. R. Prabakar, K. S. Sohn and M. Pyo, *ACS Appl. Mater. Interfaces*, 2020, **12**, 16481–16489.